1-1-1981

Simultaneous Rocket-Borne Beacon and In Situ Measurements of Equatorial Spread F - Intermediate Wavelength Results

M C. Kelley

K. D. Baker

JOURNAL OF GEOPHYSICAL RESEARCH, VOL. 86, NO. A4, PAGES 2411–2420, APRIL 1, 1981

Simultaneous Rocket-Borne Beacon and In Situ Measurements of Equatorial Spread *F*—Intermediate Wavelength Results

C. L. RINO, R. T. TSUNODA, J. PETRICEKS, AND R. C. LIVINGSTON

SRI International, Menlo Park, California 94025

M. C. KELLEY

Cornell University, Ithaca, New York 14850

K. D. BAKER

Space Measurements Laboratory, Utah State University, Logan, Utah 84322

A high-performance rocket carrying a four-frequency, phase-coherent beacon and full complement of in situ diagnostic instrumentation was launched into active equatorial spread *F* on July 17, 1979. In this paper we report the results of spectrally analyzing the beacon phase-scintillation and Langmuir probe data. By using simultaneous backscatter data from the Altair radar we were able to establish that the scintillation develops in high-density regions adjacent to the prominent plume structures and associated depletions. In these high-density regions the in situ spectra show a pronounced change in the power law slope near a spatial wavelength of 500 m. Larger scale structures admit a systematically varying power law index that is generally less than 2, in good agreement with a large body of Wideband satellite data and recently analyzed Atmospheric Explorer E data. Smaller-scale structures admit a spectral index much larger than 2. A single, overall power law near k^{-2} was found only in low-density regions that did not contribute significantly to the scintillation. The results presented here and in a companion paper suggest that refinements in the current theories of equatorial spread *F* near and above the *F* region peak are needed.

1. INTRODUCTION

On July 17, 1979, a high-performance rocket was launched during a period of severe equatorial spread *F* from Roi Namur Island located at the northern tip of the Kwajalein Atoll (9.4013°N latitude, 167.4826°E longitude, ~9° magnetic dip). The rocket carried high-resolution plasma-density probes, electric-field probes, a mass spectrometer, and a four-frequency, phase-coherent beacon to an apogee of ~600 km. In addition, the Altair radar [*Tsunoda et al.*, 1979; *Towle*, 1980; *Tsunoda*, 1980] was used to map regions of intense field-aligned backscatter, in particular the so-called backscatter plumes that generally delineate regions of depleted electron density or 'bubbles' [*Woodman and La Hoz*, 1976; *Kelley et al.*, 1976].

The launch was timed so that the rocket payload would penetrate a well-developed plume above the *F* region peak, thereby insuring that any plume-associated depletion was well into the nonlinear phase of its evolution. The experiment provided a unique opportunity to make unambiguous, quantitative comparisons among the various manifestations of equatorial spread *F*, namely severe phase and amplitude scintillation, field-aligned backscatter, electron-density depletions, and associated irregularity structures. A preliminary study has already been published [*Szuszczewicz et al.*, 1981] which supports validity of the bubble hypothesis.

The close association between equatorial gigahertz scintillation and radar backscatter plumes has been recognized for some time [*Basu et al.*, 1978; *Aarons et al.*, 1978; *Basu et al.*, 1977]. Indeed, because of this close association it has been hypothesized that intense equatorial scintillation-producing irregularities are generated by an upwelling process which brings structure into an otherwise stable topside region. *Costa and Kelley* [1976] hypothesized that the turbulent breakup of steep gradients that develop at the edges of the electron-density depletions themselves can cause the intense scintillation associated with backscatter plumes. *Basu and Basu* [1977], *Basu and Kelley* [1979], and *Rino* [1979] showed that intense scintillation could be caused not by the bubbles themselves but by extended regions of structured high density plasma on the topside.

The k^{-2} one-dimensional in situ irregularity spectral density function (SDF) that previously had been associated with equatorial spread *F* from satellite data [*Dyson et al.*, 1974] and with bottomside spread *F* using rocket data [*Kelley et al.*, 1976; *Morse et al.*, 1977] supports the notion that steep-gradients develop in the spread *F* process. Similar structures develop in low-altitude barium cloud instabilities [*Kelley et al.*, 1979]. Moreover, theoretical analyses of the nonlinear saturation of the collisional Rayleigh-Taylor and gradient drift instabilities (source mechanisms believed to produce equatorial spread *F*) also predict a k^{-2} SDF [*Chaturvedi and Ossakow*, 1977]. In fact, any electron-density configuration dominated by steep gradients must by its very nature give rise to a k^{-2} one-dimensional SDF. It should be noted that previous in situ spread *F* data are low altitude measurements and do not necessarily imply k^{-2} spectra in topside spread *F* unless the low altitude pattern is simply transported into the topside.

Remote sensing via the Wideband satellite data system has consistently shown phase spectral density functions (SDFs) as well as other independent scintillation features that imply a more shallowly sloped one-dimensional in situ SDF than k^{-2} [*Rino*, 1979; *Rino and Owen*, 1980, 1981; *Rino et al.*, 1981]. The Wideband satellite equatorial data was acquired at two stations (Ancon, Peru and Kwajalein, Marshall Islands) over a period of three years. The data from the Wideband satellite (which was in a sun-synchronous orbit) enabled us to sample

Paper number 80A1496.
0148-0227/81/080A-1496$01.00

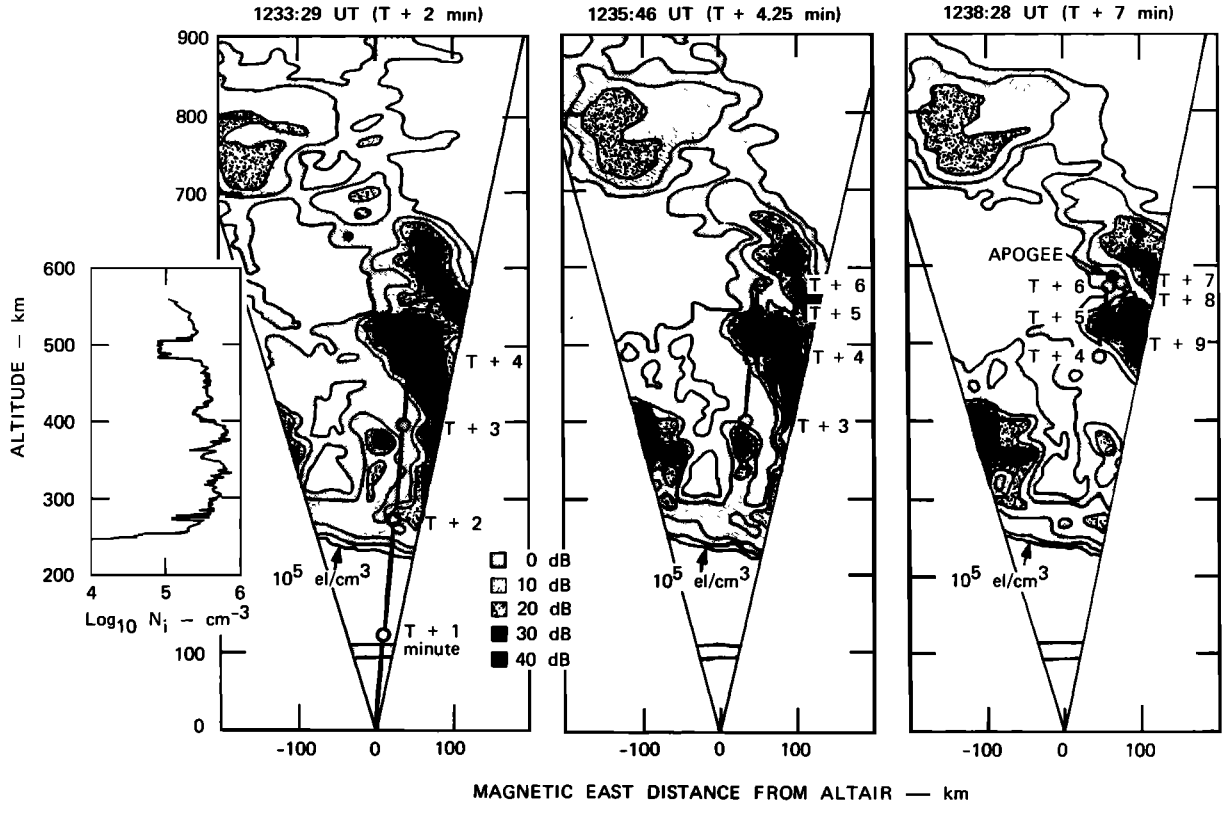

Fig. 1. Altair radar maps of field-aligned backscatter taken during the July 17, 1979, rocket launch together with Langmuir probe data.

a wide range of propagation disturbances over a 3-hour to 4-hour period, centered on local midnight.

Transionospheric propagation of radiowaves at VHF and higher frequencies causes a phase shift that is proportional to the integral of the in situ electron density along the propagation path. Thus, in interpreting the phase data, allowance must be made for this integral relationship. Moreover, the simple integral relation is strictly true only in the absence of diffraction, which is always present to some extent. Because of these subtleties, the rocket data obtained during the 1979 experiment are of considerable value in confirming the Wideband results.

In this regard, *Livingston et al.* [1981] have recently performed an analysis of a set of in situ measurements from the AE-E satellite made between 300- and 400-km altitude near Kwajalein. The data show that while the average one-dimensional spectral-index value that characterizes the in situ irregularities is near two, it varies systematically with the intensity of the irregularities. As the intensity increases, the index decreases. *Livingston et al.* [1981] showed empirically that for a one-dimensional SDF with a power law form $T_i k^{-p_i}$,

$$p_i = p_i^\circ - \eta 10 \log_{10} T_i \qquad (1)$$

with $\eta \cong 0.03$. A similar trend in the Wideband satellite phase spectral index which had been noted previously, but attributed to the aforementioned diffraction effects, was shown by *Livingston et al.* [1981] to be identical to the trend in the Atmospheric Explorer E satellite (AE-E) data.

Thus, it appears that the Wideband satellite data and the AE-E satellite data are in good agreement insofar as the spectral characterization of irregularities with spatial wavelengths greater than a few hundred meters is concerned. Indeed, by allowing for a variable spectral index, a considerable improvement of the fit to theoretically predicted scintillation coherence times was obtained [*Rino and Owen*, 1981]. Evidence of the systematic variation in the spectral index was also found in the behavior of frequency-coherence measurements [*Rino et al.*, 1981].

In this paper we present the results of spectrally analyzing the phase-scintillation and Langmuir probe data from the July 17, 1979, rocket experiment. The rocket data are shown to be in complete agreement with the Wideband and AE-E data in that they show a systematically varying spectral index for structures greater than ~500-m spatial wavelength. The Langmuir probe data can, in addition, be extended to much smaller spatial wavelengths. Furthermore, the rocket probe gives an essentially vertical profile of the irregularity structure, which complements the horizontal profiles of the AE-E and Wideband satellite data. The fact that a rocket penetrated a highly turbulent high density irregularity region for the first time has reconciled the apparent discrepancies outlined above.

Before presenting the data we note that the rocket probe provided a detailed, but brief, single data set. The rocket was, moreover launched near local midnight into conditions that can be characterized as an equatorial spread *F* decay phase. While generalizations are risky, the commonality of the results with the much larger complementary Wideband and AE-E data sets gives support to the generally representative character of the deduced structures. The local time (LT) variations in the Wideband satellite data evidently imply variations in perturbation intensity without associated structural changes.

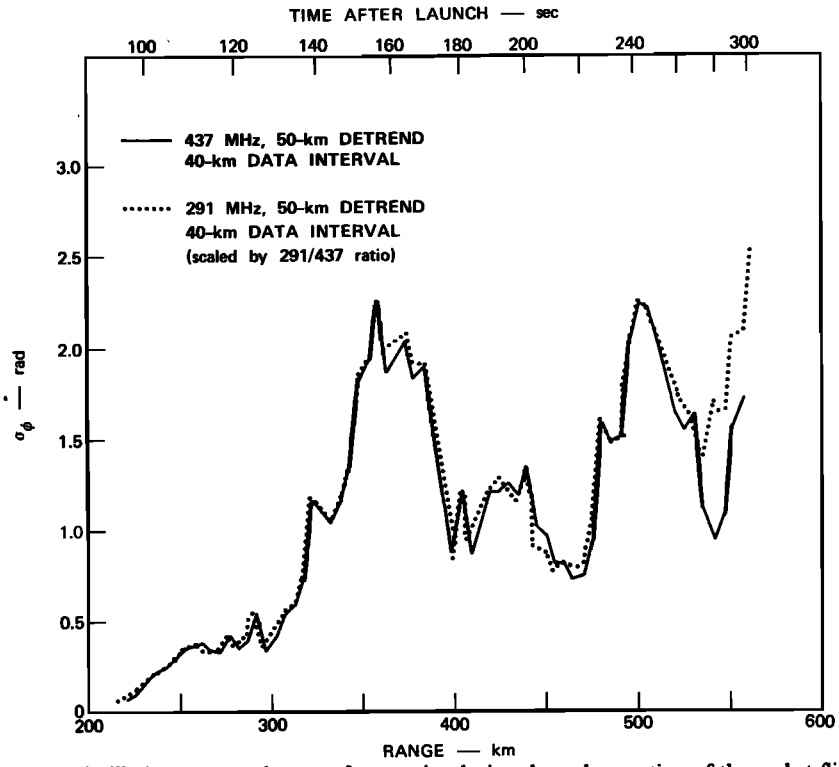

Fig. 2. RMS phase scintillation measured at two frequencies during the upleg portion of the rocket flight.

We concentrate here on the intermediate wavelength waves. Transitional and short wavelength measurements are presented in a companion paper [*Kelley et al.*, 1981].

2. The Association of Scintillation-Producing Regions With Plumes

In Figure 1 we show three Altair radar backscatter maps taken during the upleg portion of the July 17, 1979, rocket flight. The maps were made using backscatter data collected at 155.5 MHz. The strength of the field-aligned backscatter is referenced to an inocherent scatter level of 10^6 el/cm^3 (0 dB). A −10 dB contour is also given along the bottomside to show that electron densities greater than 10^5 el/cm^3 did not occur below these altitudes. Finally, the electron density profile derived from the Langmuir probe and the projection of the rocket trajectory onto the plane at which the Altair beam is perpendicular to the magnetic field are also shown in Figure 1.

We first note that between ~290 km and ~490 km (T + 2 min to T + 4 min) the rocket was generally in a region nearly devoid of field-aligned backscatter that lay adjacent to the west wall of the major plume structure (range to the rocket rather than height is used throughout the paper; note, however, that for the 84° rocket inclination angle, range and height differ by less than 1%). From the corresponding Langmuir probe data it can be seen that this is a region of high electron density and considerable large-scale structure.

Szuszczewicz et al. [1981] have analyzed the relationship between the electron density structure and the Altair field-aligned backscatter for this flight. They have noted the narrow, but highly structured region at 270 km, which is evidently associated with the west wall of the base of the plume. They find that the most intense field-aligned backscatter comes from regions with a positive electron density gradient.

In this paper, however, we are mainly interested in the structure along the propagation path to the beacon receiver at the foot of the trajectory. (The beacon antenna was located at the base of payload that an attitude control system maintained at its launch elevation angle of 84°. A variation of this scheme

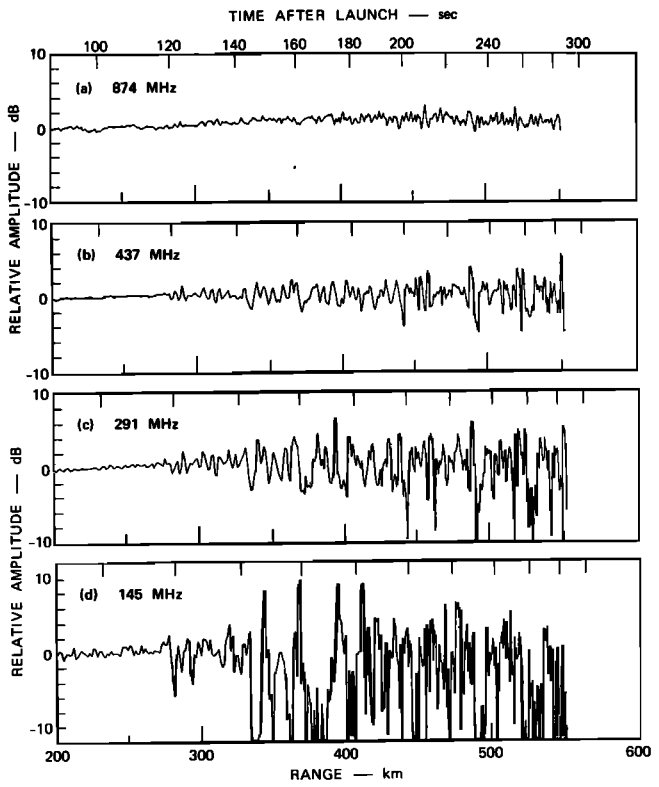

Fig. 3. Amplitude scintillation measured on the upleg portion of the rocket flight.

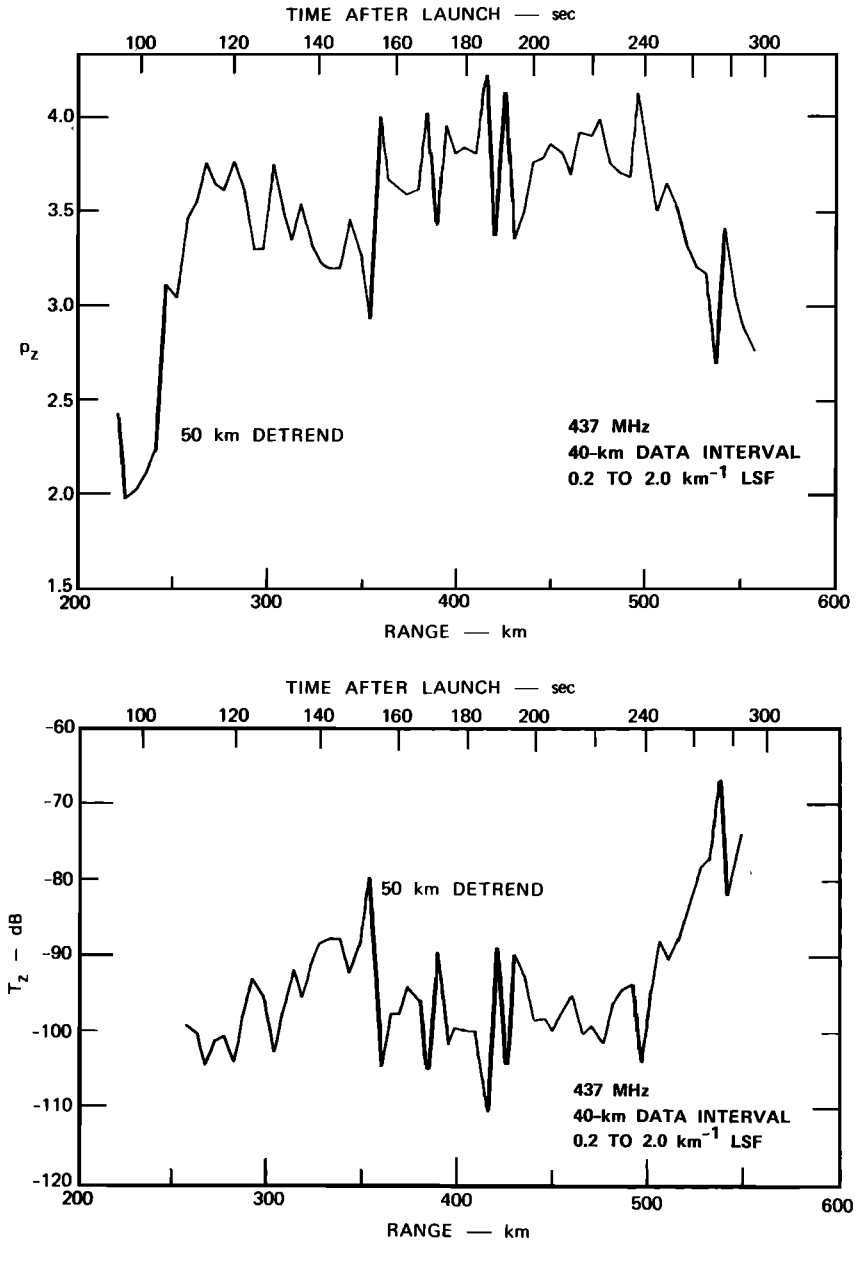

Fig. 4. Power law index and intensity parameter derived from UHF beacon phase spectra.

was evidently first used for ionospheric diagnostics by *Berning* [1951].)

By $T + 3$ min, for example, a region of enhanced field-aligned backscatter had moved into the propagation path. By the time the rocket payload had penetrated the head of the plume at ~490 km, the eastward convection carried that backscatter feature beyond the propagation path so that the propagation path again subtended a large region nearly devoid of field-aligned backscatter. From the general weakening of the backscatter strength, moreover, the plume itself was clearly in a decay phase.

In Figure 2 we show the rms phase, σ_ϕ, derived from the 437-MHz and 291-MHz rocket-beacon signals using 874 MHz as a phase reference. The data were first detrended by using a high-pass filter with a sharp, low-frequency cutoff at a spatial wavelength of 50 km. To interpret these results, consider that the differential phase $\delta\phi(t)$ is given by the integral

$$\delta\phi(t) = -r_e\lambda \int_{z_0}^{v_z t} \Delta N_e(\mathbf{v}_\perp t, \eta)\, d\eta \qquad (2)$$

where r_e is the classical electron radius, λ is the wavelength, and $\Delta N_e(\rho, z)$ is the local electron density variation. The rocket velocity vector is resolved into components along and transverse to z, v_z and $\mathbf{v}_\perp$ respectively. Because of the steep launch angle of the rocket, however, $v_z \gg v_\perp$, and we have neglected the effects of $v_\perp$ in our data interpretation. This is justified by the spectral analysis presented in section 3.

The 291-MHz data have been scaled by the wavelength ratio to verify the linear dependence on wavelength. There is also a correction for the finite reference frequency that has been applied to both the 291-MHz and 437-MHz data. The discrepancy in the rms phase measured at ranges beyond 500 km is caused by the rapid phase excursions associated with severe fading at 291 MHz.

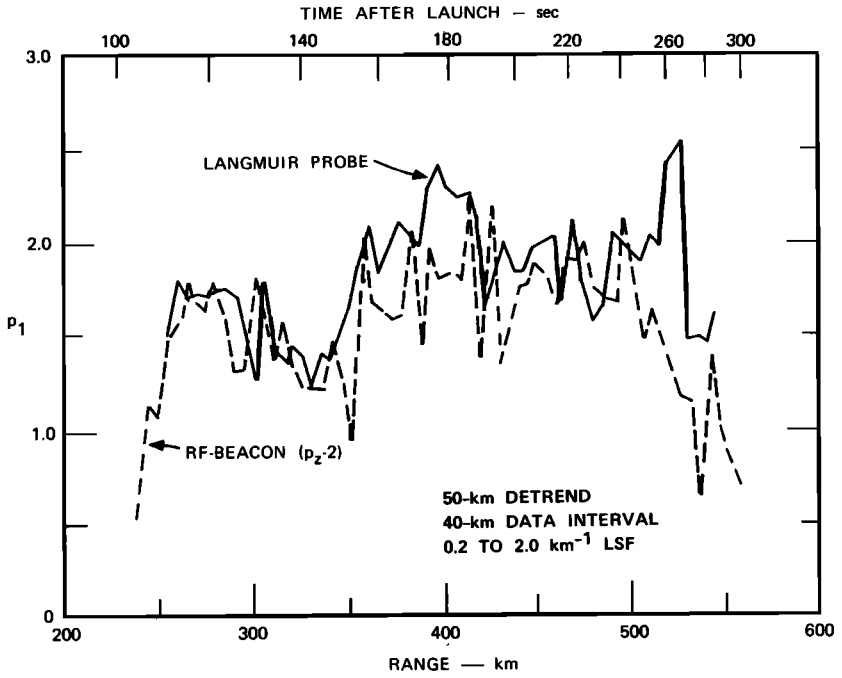

Fig. 5. Comparison of in situ and phase spectral index parameters.

From Figure 2 we see that the scintillation increases monotonically to a range of ~370 km at which first a gradual, then abrupt decrease in σ_ϕ occurs. This decrease in σ_ϕ coincides with the passage of the enhanced backscatter region into the propagation path. This implies that the backscatter region is generally devoid of large scale scintillation producing density fluctuations. Note that large relative fluctuations in low density regions do not contribute significantly to scintillation.

A second peak in phase scintillation developed as the rocket passed through 500 km. Although the rocket intercepted the head of the plume in this region, we believe that the scintillation enhancement is associated with the low-altitude regions devoid of field-aligned backscatter. This is corroborated by the different spectral characteristics of the phase and in situ irregularities in this regime, as we shall show in section 3.

To complete this section, in Figure 3 we show the amplitude scintillation on the four rocket beacon signals. The most severe scintillation at 145 MHz developed through the enhancement at 370 km, although there is a feature in the fading records near 490 km that is probably associated with the passage of the rocket into the plume head. Overall, the scintillation shows a gradual development and variation that can be approximated by homogeneous statistics over sufficiently narrow spatial intervals.

3. Spectral Analysis of Phase and In Situ Irregularity Structures

The detrended beacon phase data were first spectrally analyzed and then a log linear least squares fit was applied to the power law form $T_z k^{-p_z}$. Extreme care was taken to insure that the processing itself did not influence the extraction of the T_z and p_z parameters. A second linear detrend was applied to each data segment prior to spectral analysis to eliminate contamination due to end-point mismatch. The parameters were estimated using several detrend intervals and fits over different spatial wavenumber regimes to insure that consistent results were being obtained.

In Figure 4, we show the spectral index, p_z, and the strength parameter, T_z, derived from spectra computed over 40 km overlapping data intervals every ten kilometers along the upleg trajectory. The power law parameters were derived over the spatial wavelength interval from 0.5 km to 5.0 km. To interpret these data, we note from (2) that if $v_\perp$ is neglected and t is scaled by v_z to obtain a distance scale, then, $\delta\phi(z)$ is the integral of $r_e\lambda\Delta N_e(\rho, z)$. It follows that

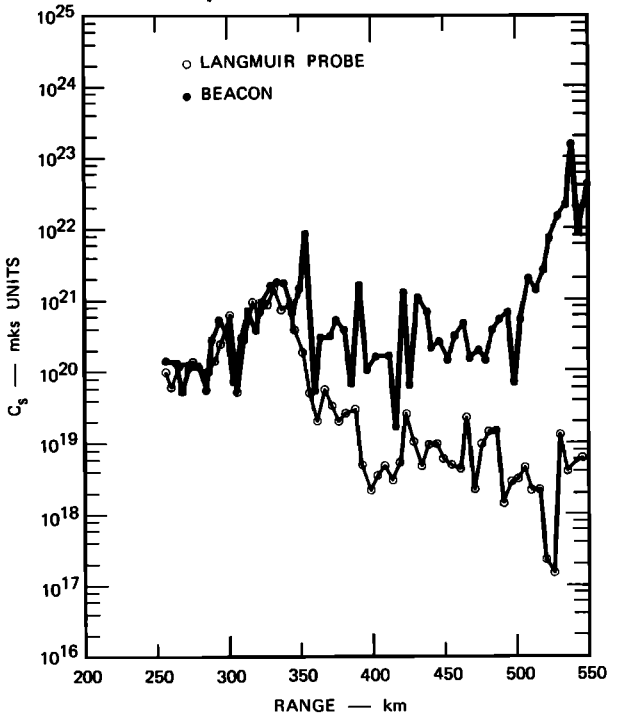

Fig. 6. Comparison of equivalent isotropic turbulence level derived from beacon-phase and Langmuir probe data.

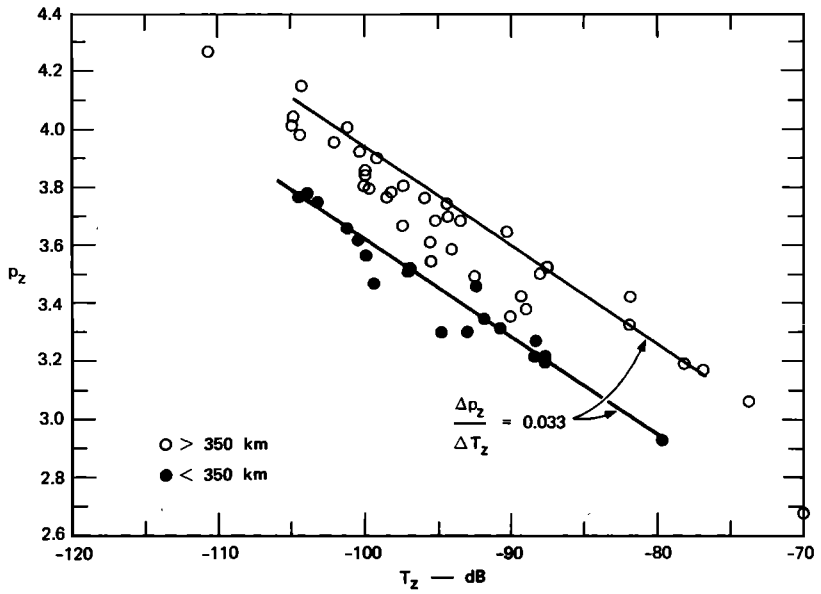

Fig. 7. Scatter diagram of phase spectral index versus turbulent strength. Closed circles are from data taken below 350 km.

$$\varphi_z(k) = r_e^2\lambda^2\frac{\varphi_1(k)}{k^2} \tag{3}$$

where $\varphi_z(k)$ is the one-dimensional phase SDF and $\varphi_1(k)$ is the corresponding in situ SDF. Unlike the more familiar phase relationship, (3) has no explicit dependence on path length or propagation geometry. If $\varphi_1(k) = T_1k^{-p_1}$, then

$$T_z = r_e^2\lambda^2T_1 \tag{4}$$

and

$$p_z = p_1 + 2 \tag{5}$$

For a k^{-2} one-dimensional in situ SDF, $p_z = 4$. From the data in Figure 4 we see that p_z is generally less than 4 and decreasing with increasing T_z to ~370 km where there is an abrupt change. As an independent check on these results, the in situ data from the Langmuir probe were processed in an identical manner to the beacon phase data to determine the in situ parameters T_1 and p_1.

In Figure 5 we show a comparison of the p_1 and p_z parameters. The quantity $p_z - 2$ is actually plotted to allow for (5). To 350 km, the agreement between these two independent measurements is nearly perfect. Above 350 km, the beacon spectral index corresponds to a value somewhat lower than the in situ spectral index. The latter is closer to the value two that is usually associated with steep gradients. This discrepancy is attributed to the fact that the beacon data are heavily weighted by the low-altitude, high-density regions where the spectral index is evidently lower than two. The low-altitude index must, however, vary as depletions pass through the propagation path. The high variability in all the spectral index measures is attributable to such spatially abrupt density structure changes.

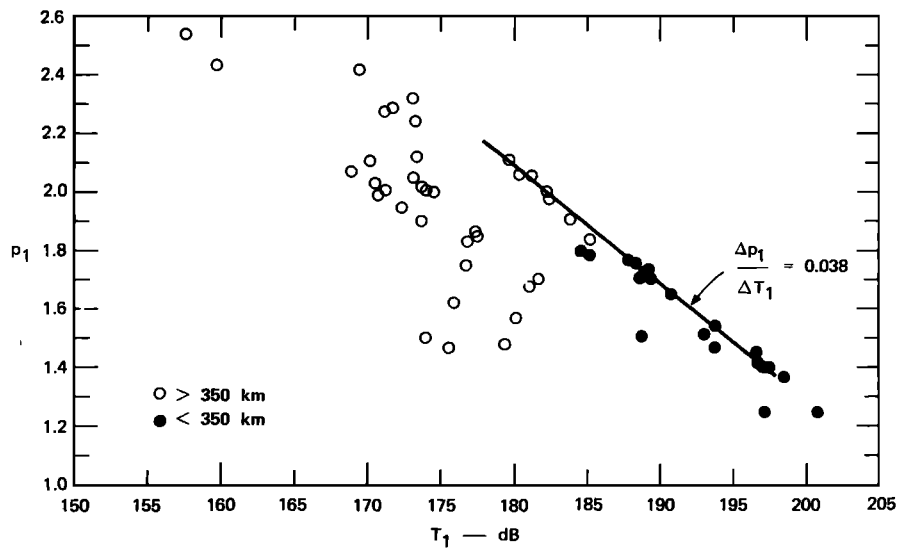

Fig. 8. Scatter diagram of Langmuir probe spectral index versus turbulent strength. Closed circles are from data taken below 350 km.

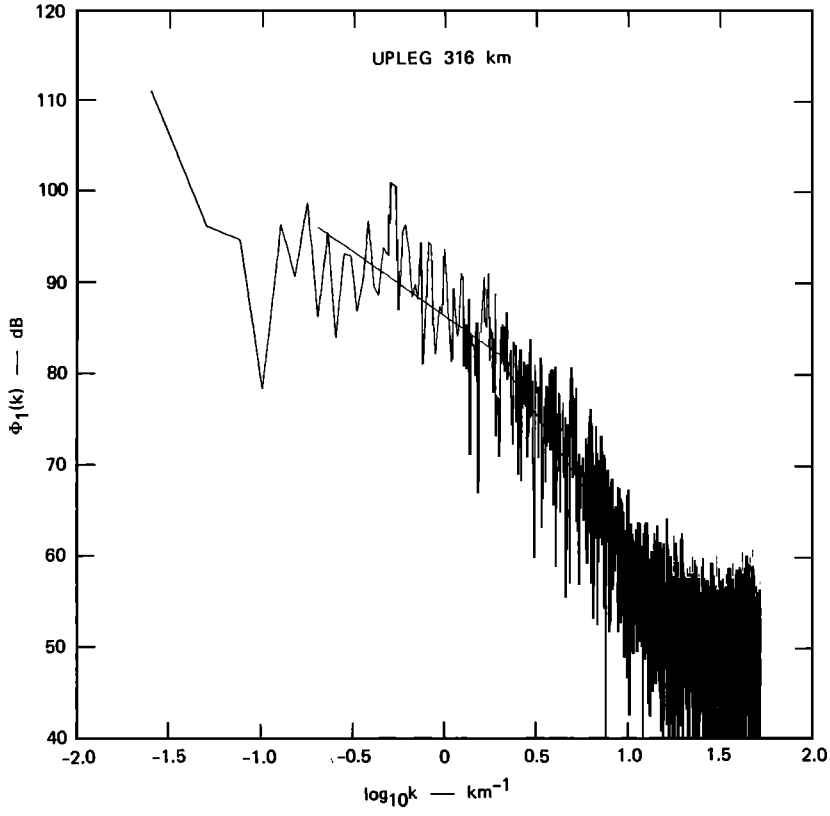

Fig. 9. Measured in situ spectral-density function at 316 km showing break near $k = 2$ km^{-1}.

To compare the spectral strength as measured by the in situ probe and the beacon, we have used the equivalent three dimensional isotropic turbulence level C_s [*Rino*, 1979]. The relationship between T_1 and C_s is

$$T_1 = \frac{C_s\Gamma(\nu - 0.5)}{(2\pi)^{2\nu+1}\Gamma(\nu + 0.5)} \tag{6}$$

where

$$\nu = (p_1 + 1)/2 \tag{7}$$

We note that T_1 is measured against wavelength in cycles per meter, whereas C_s is defined in terms of radian per meter. The beacon strength parameter can be related to C_s by using (5) and

$$\nu = (p_z - 1)/2 \tag{8}$$

The comparisons are shown in Figure 6. The Langmuir probe data provide only a relative measure of electron density. To provide an absolute density level, the probe data were initially forced to match electron density estimates derived from the Altair radar data. It was found, however, that to match the C_s values derived from the beacon phase data that an upward adjustment of 6 dB was required. In effect, the absolute value of the Langmuir probe data shown in Figure 1 is too low by a factor of two. This has since been confirmed by the pulsed plasma probe measurements reported by *Szuszczewicz and Holmes* [1981].

The agreement of the two curves to ~350 km is excellent. Above that altitude the Langmuir probe data significantly underestimate the C_s value derived from the beacon phase data. This shows that the beacon data are influenced mainly by the structured low-altitude regions of comparatively high electron density. The C_s levels observed can easily account for the gigahertz scintillation that is typically observed on equatorial Wideband satellite passes in the midnight sector [*Rino*, 1979].

To complete this section, we shall investigate more carefully the systematic variations in the power law spectral index. In Figure 7 we show a plot of p_z versus 10 $\log_{10}$ T_z. The closed circles indicate data points taken below 350 km. The rate of change of p_z per dB change in T_z as indicated by the hand-drawn straight lines is ~0.03, which is very close to the value derived by *Livingston et al.* [1981]. The data points, however, seem to separate into two regimes. The lower-altitude data (closed circles) show smaller p_z values for the same value of T_z but change at the same rate as the higher-altitude data.

The corresponding plot of p_1 versus 10 $\log_{10}$ T_1 as derived from the Langmuir probe data is shown in Figure 8. The trend in the low-altitude Langmuir probe data is virtually identical to the trend in the low-altitude beacon phase data. However, it is not clear from the Langmuir probe data that the p_1 trend persists to higher altitudes because of the large number of high-altitude data points that fall below the trend line in Figure 8. The high-altitude, in situ data are evidently tending toward a k^{-2} SDF. The data presented in section 4 give some support to this conjecture.

4. Spectral Characteristics of Structures Smaller Than 500 m

An inspection of the in situ SDF's derived from the Langmuir probe data revealed a distinct break in the SDF near a spatial wavelength of ~500 m. This wavelength is the minimum wavelength used to estimate the power law parameters that characterize the large scale regime. The break is not evi-

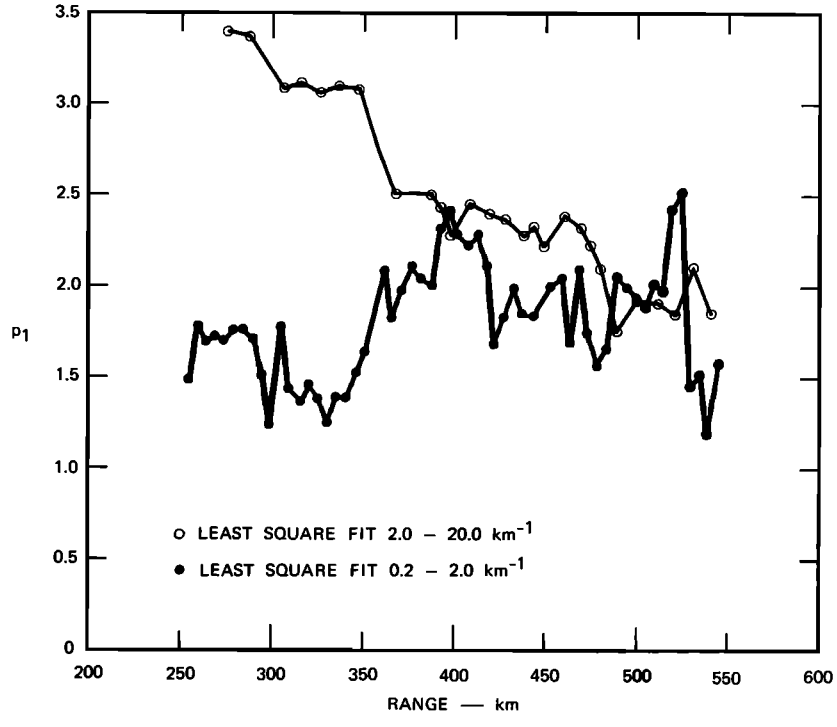

Fig. 10. Spectral indices measured over contiguous high- and low-spatial wave number regimes.

dent in the beacon data, but diffraction effects would undoubtedly mask such a feature in the phase data. In any case, we performed a separate power law least squares fit to the contiguous spectral wavelength regime below 500 m in the Langmuir probe data.

A typical spectral density function from 316-km altitude is shown in Figure 9. The power law fit to the high-frequency regime was actually performed between the spatial wave numbers corresponding to 0.5 km and 0.05 km. The power law indices for the two spectral regimes are shown in Figure 10. It can be seen that below ~370 km the high-frequency portion of the in situ SDF falls off very rapidly. Thus, there is a persistent break in the SDF near the spatial wavelength corresponding to 0.5 km up to this altitude.

Above 370 km, the in situ SDF admits a single power law representation over its medium scale to small scale regimes. In fact, given the variation in the measured indices above ~400 km, the data may well be tending toward a k^{-2} SDF as noted in section 3. The fluctuations in the spectral indices are most likely manifestations of the rapid structural changes along the flight path.

Recent analysis of high resolution AE-E data by *McClure et al.* [1980] seems to confirm these findings. Data taken near Kwajalein on the night of the July 17, 1979, rocket launch show steeply sloped spectra in high-density regions adjacent to the prominent depletions or bubbles. Spectra taken within bubbles are close to k^{-2}; moreover, many of the AE-E spectra also show a break in the power law slope near ~500 m.

From these data we conclude that in the high-density, highly structured regions of the disturbed equatorial ionosphere, the spectral regime that characterizes structures with scale sizes from tens of kilometers to tens of meters develops a distinct break near the spatial wave number corresponding to 0.5 km. The larger structures are characterized by a comparatively shallow power law spectral slope that varies systematically with spectral strength. The smaller scale structures are characterized by a much steeper power law spectral slope that also seems to vary with spectral strength. At higher altitudes where the perturbation levels are much smaller, a single power law near k^{-2} characterizes the SDF over the entire spectral regime corresponding to scale sizes greater than a few tens of meters.

More recent high resolution spectral analyses within the bottomside depletion at 270 km show a $k^{-2.5}$ SDF [*Szuszczewicz and Holmes,* 1980]. Because these spectra were evaluated over 2.4 km intervals, however, they exclude the larger scale structures that evidently give rise to the more shallowly sloped SDF's. Alternatively, the low density region where the spectra were taken may genuinely be characterized by a k^{-2} SDF.

5. SUMMARY AND DISCUSSION

In this paper we have presented the results of simultaneous measurements of equatorial spread *F* using a rocket-borne phase-coherent beacon and an in situ electron density probe. Spectral analysis of the rocket data confirms earlier results deduced indirectly from Wideband satellite data and, more recently, directly from AE-E satellite data. The rocket data, however, have provided an altitude profile of the irregularity structures. Together with backscatter data from the Altair radar, these data have provided new insight into the interrelationships among the various manifestations of equatorial spread *F* and its spectral characterization.

The data presented and reviewed in this paper support the following conclusions:

1. The ionospheric regions that cause the most intense equatorial scintillation are high plasma density regions through the *F* region peak that lie adjacent to the prominent depletions associated with backscatter plumes. (*Tsunoda* [1981] has shown evidence of structure favoring the west side

of plumes and attributed the effect to an eastward neutral wind.)

2. Specific diffraction effects associated with propagation through large depletions are highly localized and difficult to detect in a background of scintillation generated by adjacent regions (Figure 3).

3. The scintillation effects are almost fully accounted for by the structure above but within a hundred kilometers of the bottom of the F layer. This is most readily seen by comparing the equivalent isotropic turbulence levels as measured by the beacon and the Langmuir probe (Figure 6).

4. The average spectral characterization of the most intense irregularities with scale sizes between several hundred meters and several tens of kilometers follows the one-dimensional power law, $T_1 k^{-p_1}$. The spectral index, p_1, decreases with increasing T_1 at a rate between 0.03 and 0.04 units per dB change in T_1, but generally falls below the value $p_1 = 2$. This effect has been verified independently by Wideband satellite phase scintillation data and AE-E data.

5. In the most highly disturbed regions the one-dimensional in situ SDF's show a pronounced break in their power law slopes near the spatial wave number corresponding to a wavelength of 0.5 km. The spatial wave number regime corresponding to spatial wavelengths between several hundred meters and several tens of meters admits a power law characterization with an index much larger than 2. As with the large-scale regime the index is variable.

6. In the higher altitude and lower-density regions, also possibly in lower-density regions within the depletions, the spectral characterization of the irregularities admits a single power characterization with a one dimensional index near the usually reported value $p_1 = 2$.

As we noted in the introduction, the rocket data were taken near local midnight when equatorial spread F is much weaker than it is in the post sunset period. Moreover, the plume intercepted by the rocket was itself in a decay phase. We believe, however, that the only effect this has on the structure is to produce smaller turbulence levels. This conjecture is based on the consistency of the structures observed by the Wideband satellite and AE-E over extended time periods.

As to why the dominant irregularities with scale sizes from tens of meters to tens of kilometers should admit a variable two-component power law spectral characterization, we consider the extensive work that has been done in two-dimensional fluid turbulence. *Kelley and Ott* [1978] have discussed the applicability of the theory to equatorial spread F. A well-established feature of the theory is an upward (toward longer wavelengths) cascade of energy in the velocity field and a downward cascade of enstrophy about an initially unstable mode—the stirring scale in Kelley and Otts' terminology. The stirring scale is evidenced in the velocity power spectrum as a break between a shallowly sloped region where the upward cascade takes place and a more steeply sloped downward cascade region. The region in which we observe dual-sloped spectra and strong turbulence, namely, the region near and above the F peak, is where Kelley and Ott predicted enhanced velocity turbulence due to the breaking up of bubble velocities via electrostatic discharge into the background medium between and behind bubbles.

The existing theory unfortunately does not predict density fluctuation spectra such as reported here. Dynamical arguments together with dimensional arguments can be used to determine the power law index for the density spectrum under certain assumptions. The simplest extension of the theory to yield a density spectrum stems from assuming it to be a passive scalor [*Kelley and Ott,* 1978], and predicts a k^{-1} one-dimensional spectrum in the downward cascade regime, whereas our data show a much steeper slope. In fact, intermediate and short wavelength data discussed in the companion paper [*Kelley et al.,* 1981] show that the density is probably not a passive scalor but part of a driving mechanism, namely, the drift wave instability. Moreover, the theory does not explain the variability in the slope or the 500-m scale itself. It is interesting to note, however, that 500 m is a typical dimension for the finger-like striations that develop in barium clouds [*Keskinen et al.,* 1980*a*].

Finally, we note that while virtually all simulations of the Rayleigh-Taylor and/or gradient drift instabilities favor a one-dimensional spectrum near k^{-2} [*Keskinen et al.,* 1980*b*; *Scannapieco and Ossakow,* 1976], a question of adequate resolution remains. In the rocket data, for example, we computed spectra with a 10-m sample interval over 40-km intervals covering several hundred kilometers in altitude. *Scannapieco and Ossakow* [1976] reported a single spectrum for their entire bubble simulation. The high spatial resolution results of *Keskinen et al.* [1980*b*], while achieving a resolution of 1.5 m, encompassed only a few striations. Furthermore, if drift waves are important, a finite $k_{\parallel}$ is essential to the process and must be included in the simulation. Rapid progress is being made in such calculations and we believe that the simulations have the potential to verify the results presented in this paper.

Acknowledgments. This work was supported at SRI International by the Defense Nuclear Agency under contracts DNA001-79-C-0128 and DNA001-80-C-0009 and at Utah State University under contract DNA001-79-C-0133. The authors gratefully acknowledge the assistance of R. H. Scofield in acquiring the rocket beacon data.

REFERENCES

Aarons, J., J. Buchau, S. Basu, and J. P. McClure, The localized origin of equatorial F region irregularity patches, *J. Geophys. Res.*, *83*, 1659, 1978.

Basu, S., and S. Basu, Correlated measurements of scintillations and in situ F-region irregularities from Ogo 6, *Geophys. Res. Lett.*, *3*, 681, 1976.

Basu, S., and M. C. Kelley, A review of recent observations of equatorial scintillations and their relationship to current theories of F region irregularity generation, *Radio Sci.*, *14*, 471, 1979.

Basu, S., J. Aarons, J. P. McClure, C. La Hoz, A. Bushby, and R. F. Woodman, Preliminary comparisons of VHF radar maps of F-region irregularities with scientillations in the equatorial region, *J. Atmos. Terr. Phys.*, *39*, 1251, 1977.

Basu, S., S. Basu, J. Aarons, J. P. McClure, and M. D. Cousins, On the coexistence of kilometer- and meter-scale irregularities in the nighttime equatorial F region, *J. Geophys. Res.*, *83*, 4219, 1978.

Berning, W. W., Charge densities in the ionosphere from radio Doppler data, *J. Meteorol.*, *8*, 176, 1951.

Chaturvedi, P, K., and S. L. Ossakow, Nonlinear theory of the collisional Rayleigh-Taylor instability in equatorial spread, *Geophys. Res. Lett.*, *4*, 558, 1977.

Costa, E., and M. C. Kelley, Calculations of equatorial scintillations at VHF and gigahertz frequencies based on a new model of the disturbed equatorial ionosphere, *Geophys. Res. Let.*, *3*, 677, 1976.

Dyson, P. L., J. P. McClure, and W. B. Hanson, In situ measurements of the spectral characteristics of F-region ionospheric irregularities, *J. Geophys. Res.*, *79*, 1497, 1974.

Kelley, M. C., and E. Ott, Two-dimensional turbulence in equatorial spread F, *J. Geophys. Res.*, *83*, 4369, 1978.

Kelley, M. C., G. Haerendel, H. Kappler, A. Valenzuela, B. B. Balsley, D. A. Carter, W. L. Ecklund, C. W. Carlson, B. Hausler, and R. Torbert, Evidence for a Rayleigh-Taylor type instability and up-

welling of depleted density regions during equatorial spread-*F*, *Geophys. Res. Lett.*, *3*, 448, 1976.

Kelley, M. C., D. K. Baker, and J. C. Ulwick, Late time barium cloud striations and their relationships to equatorial spread *F*, *J. Geophys. Res.*, *84*, 1898, 1979.

Kelley, M. C., R. Pfaff, K. D. Baker, J. C. Ulwick, R. C. Livingston, C. L. Rino, and R. T. Tsunoda, Simultaneous rocket probe and radar measurements of equatorial spread *F*—Transitional and short wavelength results, submitted to *J. Geophys. Res.*, 1981.

Keskinen, M. J., B. E. McDonald, and S. L. Ossakow, Preliminary numerical study of the outer scale size of ionospheric plasma cloud striations, *J. Geophys. Res.*, *85*, 2349, 1980*a*.

Keskinen, M. J., S. L. Ossakow, and P. K. Chaturvedi, Preliminary report of numerical simulations of intermediate wavelength collisional Rayleigh-Taylor instability in equatorial spread *F*, *J. Geophys. Res.*, *85*, 1775, 1980*b*.

Livingston, R. C., C. L. Rino, J. P. McClure, and W. B. Hanson, Spectral characteristics of medium-scale equatorial *F* region irregularities, *J. Geophys. Res.*, in press, 1981.

McClure, J. P., C. E. Valladares, W. B. Hanson, and R. T. Tsunoda, Comparison of large-scale quasi-periodic Rayleigh-Taylor plasma instabilities and small-scale instability processes associated with the 1979 Kwajalein rocket (abstract), *Eos Trans. AGU*, *61*, 314, 1980.

Morse, F. A., B. C. Edgar, H. C. Koons, C. J. Rice, W. J. Heikkila, J. H. Hoffman, B. A. Tinsley, J. D. Winningham, A. B. Christensen, R. F. Woodman, J. Pomalaza, and R. N. Teizeira, Equion, an equatorial ionospheric irregularity experiment, *J. Geophys. Res.*, *82*, 578, 1977.

Rino, C. L., A power-law phase screen model for ionospheric scintillation, 1, Weak scatter, *Radio Sci.*, *14*, 1135, 1979.

Rino, C. L., and J. Owen, The time structure of transionospheric radiowave scintillation, *Radio Sci.*, 15, 479, 1980.

Rino, C. L., and J. Owen, On the temporal coherence loss of strongly scintillating signals, *Radio Sci.*, *16*, 31, 1981.

Rino, C. L., V. H. Gonzalez, and A. R. Hessing, Coherence bandwidth loss in transionospheric radio propagation, *Radio Sci.*, *16*, 245, 1981.

Scannapieco, A. J., and S. L. Ossakow, Nonlinear equatorial spread-*F*, *Geophys. Res. Lett.*, *3*, 451, 1976.

Szuszczewicz, E. P., and J. C. Holmes, Equatorial spread *F*: 'In situ' measurements of electron density temperature and density fluctuation power spectra, submitted to *Geophys. Res. Lett.*, 1981.

Szuszczewicz, E. P., R. T. Tsunoda, R. Narcisi, and J. C. Holmes, Coincident radar and rocket observations of equatorial spread *F*, *Geophys. Res. Lett.*, in press, 1981.

Towle, D. M., VHF and UHF radar observations of equatorial ionospheric irregularities and background densities, *Radio Sci.*, *15*, 71, 1980.

Tsunoda, R. T., On the spatial relationship of 1-m equatorial spread *F* irregularities and plasma bubbles, *J. Geophys. Res.*, *85*, 185, 1980.

Tsunoda, R. T., Time evolution and dynamics of equatorial backscatter plumes, 1, Growth phase, *J. Geophys. Res.*, *86*, 139, 1981.

Tsunoda, R. T., M. J. Baron, J. Owen, and D. M. Towle, Altair: An incoherent scatter radar for equatorial spread *F* studies, *Radio Sci.*, *14*, 1111, 1979.

Wernik, A. W., C. H. Liu, and K. C. Yeh, Model computations of radio wave scintillation caused by equatorial ionospheric bubbles, *Radio Sci.*, 15, 559, 1980.

Woodman, R. F., and C. La Hoz, Radar observations of *F* region equatorial irregularities, *J. Geophys. Res.*, *81*, 5447, 1976.

(Received July 21, 1980;
revised October 20, 1980;
accepted October 21, 1980.)